18. VPDB is a terrestrial isotopes standard.
19. P. B. Niles, W. V. Boynton, J. H. Hoffman, D. W. Ming, D. Hamara, *Science* **329**, 1334–1337 (2010).
20. V. A. Krasnopolsky, J. P. Maillard, T. C. Owen, R. A. Toth, M. D. Smith, *Icarus* **192**, 396–403 (2007).
21. D. D. Bogard, P. Johnson, *Science* **221**, 651–654 (1983).
22. R. H. Carr, M. M. Grady, I. P. Wright, C. T. Pillinger, *Nature* **314**, 248–250 (1985).
23. H. Y. McSween Jr., *Meteoritics* **29**, 757–779 (1994).
24. U. Ott, *Geochim. Cosmochim. Acta* **52**, 1937–1948 (1988).
25. U. Ott, F. Begemann, *Meteoritics* **20**, 721 (1985).
26. S. V. S. Murty, R. K. Mohapatra, *Geochim. Cosmochim. Acta* **61**, 5417–5428 (1997).
27. D. D. Bogard, D. H. Garrison, *Meteorit. Planet. Sci.* **33** (suppl.), 19 (1998).
28. A. H. Treiman, J. D. Gleason, D. D. Bogard, *Planet. Space Sci.* **48**, 1213–1230 (2000).
29. T. Owen, A. Bar-Nun, *AIP Conf. Proc.* **341**, 123–138 (1994).
30. T. D. Swindle, *AIP Conf. Proc.* **341**, 175 (1994).
31. T. D. Swindle, J. H. Jones, *J. Geophys. Res.* **102**, 1671 (1997).
32. Details of measurement procedures and treatment of uncertainties are provided in the supplementary materials on *Science* Online.
33. The turbomolecular pumps on SAM are expected to provide a more stable pressure of noble gas in the mass spectrometer ion source compared with the small ion pumps used on Viking.
34. C. R. Webster *et al.*, *Science* **341**, 260–263 (2013).
35. A. J. T. Jull, C. J. Eastoe, S. Cloudt, *J. Geophys. Res.* **102**, 1663 (1997).
36. B. M. Jakosky, R. O. Pepin, R. E. Johnson, J. L. Fox, *Icarus* **111**, 271–288 (1994).
37. D. H. Garrison, D. D. Bogard, *Meteorit. Planet. Sci.* **35** (suppl.), A58 (2000).
38. D. D. Bogard, R. N. Clayton, K. Marti, T. Owen, G. Turner, *Space Sci. Rev.* **96**, 425–458 (2001).
39. R. C. Wiens, R. O. Pepin, *Geochim. Cosmochim. Acta* **52**, 295–307 (1988).
40. D. Bogard, F. Horz, *Meteoritics* **21**, 337 (1986).
41. R. O. Pepin, *Nature* **317**, 473–475 (1985).
42. R. O. Pepin, *Icarus* **111**, 289–304 (1994).
43. T. Owen, A. Bar-Nun, *Icarus* **116**, 215–226 (1995).
44. P. R. Mahaffy *et al.*, *J. Geophys. Res. Planets* **105**, 15061–15071 (2000).
45. B. M. Jakosky, J. H. Jones, *Rev. Geophys.* **35**, 1–16 (1997).

Supplementary Materials

www.sciencemag.org/cgi/content/full/341/6143/263/DC1
Materials and Methods
Tables S1 and S2
References (*46*, *47*)
MSL Science Team Author List

18 March 2013; accepted 4 June 2013
10.1126/science.1237966

Ice-Shelf Melting Around Antarctica

E. Rignot,[1,2]* S. Jacobs,[3] J. Mouginot,[1] B. Scheuchl[1]

We compare the volume flux divergence of Antarctic ice shelves in 2007 and 2008 with 1979 to 2010 surface accumulation and 2003 to 2008 thinning to determine their rates of melting and mass balance. Basal melt of 1325 ± 235 gigatons per year (Gt/year) exceeds a calving flux of 1089 ± 139 Gt/year, making ice-shelf melting the largest ablation process in Antarctica. The giant cold-cavity Ross, Filchner, and Ronne ice shelves covering two-thirds of the total ice-shelf area account for only 15% of net melting. Half of the meltwater comes from 10 small, warm-cavity Southeast Pacific ice shelves occupying 8% of the area. A similar high melt/area ratio is found for six East Antarctic ice shelves, implying undocumented strong ocean thermal forcing on their deep grounding lines.

The Antarctic Ice Sheet and its 58-m sea level equivalent (*1*) is buttressed along most of its periphery by floating extensions of land ice called ice shelves and floating ice tongues (Fig. 1). Ice shelves cover an area >1.561 million km^2, comparable in size to the Greenland Ice Sheet, and fringe 75% of Antarctica's coastline while collecting 20% of its snowfall over 11% of its area (*2*, *3*). These features are nourished by the inflow of continental ice from grounded glaciers, surface accumulation, and freezing of marine ice on their undersides. They lose mass to iceberg calving and basal melting along with topside sublimation and wind drift. Ice shelves exert considerable control on glacier stability and Antarctic Ice Sheet mass balance (*4*–*6*) and play important roles in ocean stratification and bottom water formation (*7*).

The traditional view of ablation from Antarctic ice shelves has been that it occurs mostly by iceberg calving, with basal melting only contributing 10 to 28% of the total mass loss (*3*–*6*). Estimates of ice-shelf meltwater production derived from oceanographic data (*8*–*10*, e.g.) are impractical for synoptic circumpolar coverage. Numerical simulations of ice-ocean interactions extend from individual ice shelves to circumpolar models at various resolutions, but comparisons with observations are limited, and estimates of total ice-shelf meltwater production have varied from 357 to 1600 gigatons per year (1 Gt = 10^{12} kg) (*3*, *7*, *11*). Glaciological estimates have focused on few ice shelves (*6*, *12*, *13*) or near a fraction of glacier grounding lines (*14*) due to incomplete velocity and thickness mapping.

Here, we present more accurate, higher-resolution glaciological estimates of ice-shelf melting around the entire continent. At any point on an ice shelf of thickness H and velocity vector $\mathbf{v}$, the rate of ice-shelf thickening $\partial H/\partial t$ equals the sum of net surface mass balance *SMB* minus net basal melting B minus the lateral divergence in volume flux $H\mathbf{v}$ (*15*). A negative value of B indicates the freeze-on of marine ice. The calculation of volume flux divergence on a point per point basis yields the distribution of freeze/melt (Fig. 1). The integration of the total inflow and outflow within the ice-shelf perimeters yields the area-average melt rate and total meltwater production (Table 1).

For *SMB*, we use output products from the Regional Atmospheric and Climate Model RACMO2 (*16*), which is forced at the lateral boundary and sea surface by global reanalyses of the European Centre for Medium-Range Weather Forecasts. RACMO2 includes surface meltwater retention due to refreezing, evaporation, wind drift, and sublimation. The products have been validated with field data and an error propagation analysis (*17*) to a precision of 7 to 25%, average 10%, depending on location. We use the average *SMB* for the years 1979 to 2010 to represent a longer-term state.

Ice-shelf thickness is from Operation IceBridge (OIB) (*18*, *19*) and BEDMAP-2 (*1*) (fig. S1, supplementary materials). It combines direct measurements from radio-echo sounding, with indirect estimates from altimetry-derived ice-shelf surface elevation assuming hydrostatic equilibrium with a nominal precision of 15 to 50 m (*20*). Flux gates are selected at the location of Interferometric Synthetic Aperture Radar (InSAR)–derived grounding lines, which are more precise than those derived from photogrammetric techniques or visible imagery (*21*), with accompanying impacts on estimates of volume fluxes. Ice-front flux gates are at the seaward limit of the volume flux data, within 1 to 3 km of ice-front positions digitized from a 150-m spacing mosaic of Advanced Land Observing System (ALOS) Polarimetric SAR (PALSAR) data for the years 2007 and 2008.

Ice-shelf flow vector velocities are from InSAR data collected in 2007 and 2008 and processed at 450-m spacing (*22*). The average precision in speed is 4 m/year and 1.7° in direction (fig. S2). In the absence of vertical shear on floating ice, the surface-derived velocity is equivalent to a depth-averaged velocity. We surveyed 99.5% of Antarctic ice-shelf area in 2007 and 2008 (Table 1), or 1.554 million km^2, excluding a few smaller ice shelves where ice thickness is not well known (table S1). Drainage boundaries between ice shelves, including the eastern and western Ross, are defined by flow vector direction. Ice rises and islands are excluded from the ice-shelf area estimates but included in the *SMB* calculation.

Ice-shelf thickening $\partial H/\partial t$ for the period 2003 to 2008 is calculated using the procedure in (*23*), with an error dependent on firn depth corrections (fig. S3). The results are combined with *SMB* and the flux divergence to calculate B, with a precision dominated by uncertainties in

[1]Department of Earth System Science, University of California, Irvine, CA 92697, USA. [2]Jet Propulsion Laboratory, Pasadena, CA 91109, USA. [3]Lamont-Doherty Earth Observatory, Columbia University, Palisades, NY 10964, USA.

*Corresponding author. E-mail: erignot@uci.edu

ice-front thickness and firn depth corrections (table S1). We also calculate the results for $\partial H/\partial t = 0$, i.e., no ice-shelf thickness change, to obtain a reference rate B_{ss} corresponding to the amount of freezing or melting that would be required to maintain an ice shelf in "steady state" for 2007 and 2008 (fig. S4).

The freeze/melt distribution confirms that basal melting is strongest near the grounding zones of major glaciers and along the ice fronts of some of the largest ice shelves, especially Ronne (Fig. 1). Ice-shelf melting decreases away from grounding lines and becomes negative (accretion of marine ice) on all large ice shelves and some smaller ice shelves. This general pattern of melting and freezing beneath ice shelves is well understood (*4*–*6*, *15*) and is governed by the Coriolis-influenced transport and vertical mixing of ocean heat, the pressure dependence of the freezing point of seawater, and the sea floor and cavity morphology. On some large ice shelves, freezing is concentrated on the western sides, consistent with an oceanic circulation during which seawater is first cooled, freshened, and made more buoyant by melting.

The highest melt rates are detected in the Southeast Pacific sector of the Antarctic Peninsula and West Antarctica, from the northern end of George VI to the western end of Getz Ice Shelf. On slow-moving to nearly stationary ice shelves like the Wilkins, George VI, Abbot, and Sulzberger, basal melting entirely consumes the inflow of individual glaciers within a few km of their grounding zones. High melt rates are also revealed in the grounding zones of the Amery, Moscow University, Shackleton, and Totten in East Antarctica.

In contrast, low melt rates are found under the largest ice shelves—for example, the Ross West—except near deep grounding lines. Maximum grounding-line depth is only 0.9 km under the Ross West but 2.1 km under the Filchner and Ronne, 1.8 km under the Ross East, and 2.4 km under the Amery (*1*). Each additional 100 m adds 0.076°C to the thermal driving of seawater that may have started out near the sea-surface freezing point. Differences in observed melt rate may also be accentuated by variations in flushing time and tidal activity (*24*).

Total ice inflow and outflow for each ice shelf is summarized in Fig. 1 and Table 1. Ice-front flux is a proxy for, but not identical to, iceberg calving, which occurs at irregular time intervals ranging from days to decades. The higher basal melting near some ice-shelf fronts (*12*, *25*) results from stronger tidal currents and mixing, especially in combination with a shallow water column (*24*), as along the eastern front of Ronne [150 ± 50 m in (*1*) versus 350 ± 100 m for Ross or 500 ± 250 m for Filchner]. Ice-front fluxes may overestimate iceberg calving where near-ice-front melting is substantial and calving is infrequent; conversely, large icebergs may on average be thicker than the ice front, in which case ice-front fluxes underestimate calving.

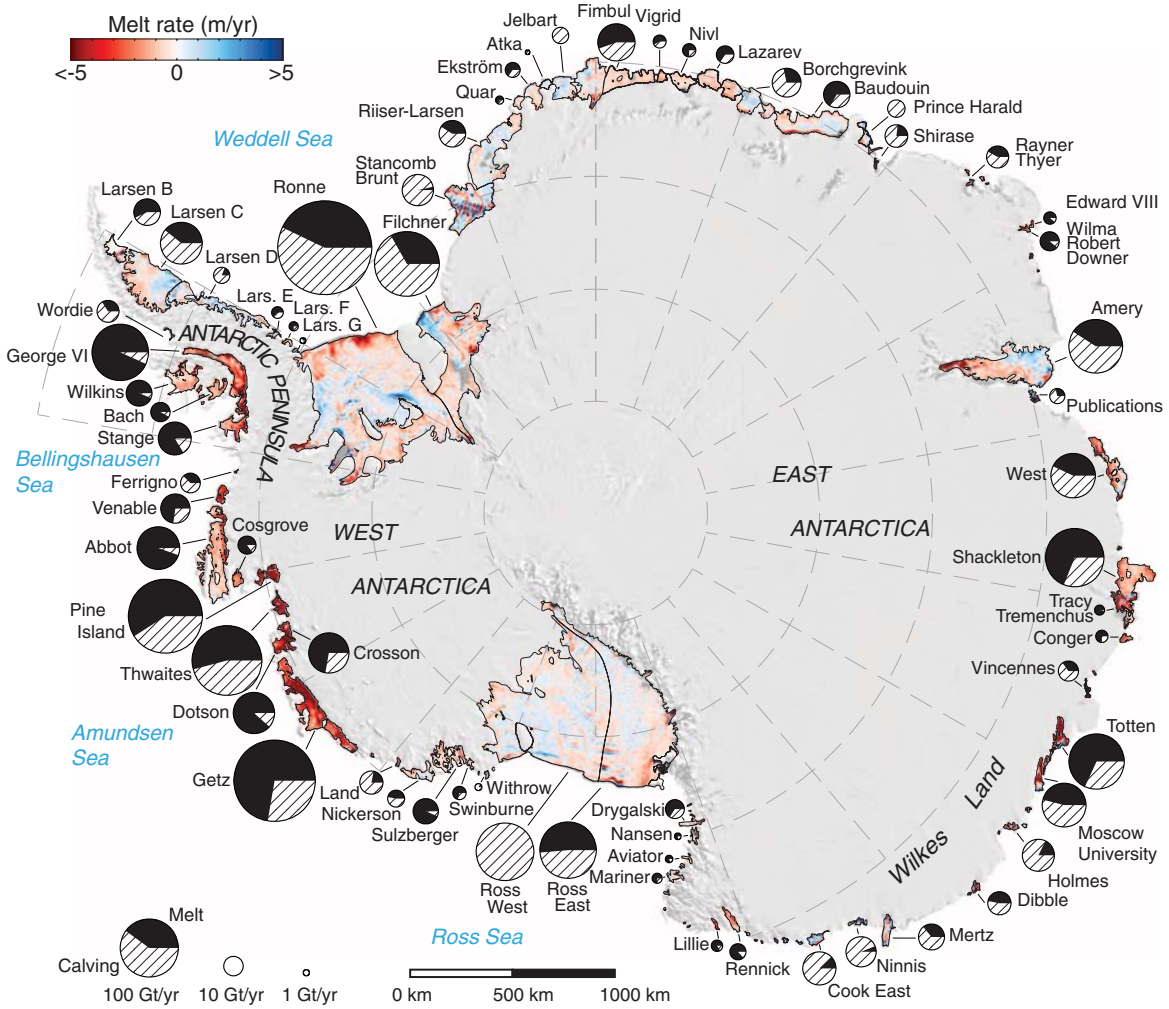

Fig. 1. Basal melt rates of Antarctic ice shelves. Color coded from <–5 m/year (freezing) to >+5 m/year (melting) and overlaid on a 2009 Moderate Resolution Imaging Spectroradiometer mosaic of Antarctica. Ice-shelf perimeters in 2007 and 2008, excluding ice rises and ice islands, are thin black lines. Each circle graph is proportional in area to the mass loss from each shelf, in Gt/year, partitioned between iceberg calving (hatch fill) and basal melting (black fill). See Table 1 and table S1 for additional details on ice-shelf locations, areas, and mass balance components.

Table 1. Meltwater production of Antarctic ice shelves, with ice shelves named in Fig. 1. Areas in square kilometers exclude ice rises and islands. Grounding-line flux (GL), surface mass balance (SMB), ice-front (proxy for calving) flux (Ice Front), ice-shelf mass gain ($\partial H/\partial t$ in water mass equivalent), and basal meltwater production in Gt/year, with area-average basal melt rate in meters of water per year indicated in parenthesis. Total Antarctica in the last row includes nonsurveyed coastal sectors. Ice-shelf names are from United States Geological Survey and (*3*). Surveyed ice-shelf mass loss of 287 ± 89 Gt/year in 2003 to 2008 ($\partial H/\partial t$) is 28 ± 9% higher than that required to maintain the ice shelves in steady state for 2003 to 2008. *, Larsen B data (velocity, thickness) before the 2002 collapse; thinning rate from the remnant part of the ice shelf only. Additional details in table S1.

Name	Area km^2	GL Gt/year	SMB Gt/year	Ice front Gt/year	$\partial H/\partial t$ Gt/year	Basal melt Gt/year (m/year)
Larsen G	412	0.9 ± 0.2	0.1 ± 0	0.7 ± 1	0.0 ± 0	0.3 ± 0.2 (0.71 ± 0.6)
Larsen F	828	1.5 ± 0.3	0.3 ± 0.1	0.6 ± 1	−0.7 ± 0.5	1.2 ± 0.4 (1.4 ± 0.5)
Larsen E	1,184	3.6 ± 0.7	0.4 ± 0.1	1.5 ± 1	1.1 ± 0.7	1.4 ± 1 (1.2 ± 0.9)
Larsen D	22,548	18.5 ± 4	9.8 ± 2	6.3 ± 1	20.5 ± 14	1.4 ± 14 (0.1 ± 0.6)
Larsen C	46,465	29.6 ± 3	23.8 ± 4	31.3 ± 3	1.4 ± 67	20.7 ± 67 (0.4 ± 1)
Larsen B*	6,755	13.6 ± 3	3.0 ± 0.6	8.9 ± 1	−4.5 ± 13	12.2 ± 14 (1.8 ± 2)
Wordie	277	13.8 ± 1	0.3 ± 0	7.6 ± 3	−0.1 ± 0	6.5 ± 3 (23.6 ± 10)
Wilkins	12,866	7.8 ± 2	8.3 ± 2	0.7 ± 0.4	−3.4 ± 16	18.4 ± 17 (1.5 ± 1)
Bach	4,579	5.4 ± 1	1.8 ± 0.3	0.8 ± 0.2	−4.0 ± 0.3	10.4 ± 1 (2.3 ± 0.3)
George VI	23,434	68.2 ± 5	12.7 ± 2	5.7 ± 1.2	−13.8 ± 16	89.0 ± 17 (3.8 ± 0.7)
Stange	8,027	21.0 ± 3	6.0 ± 1	4.6 ± 0.8	−5.6 ± 5	28.0 ± 6 (3.5 ± 0.7)
Antarctic Peninsula	127,375	184 ± 26	66 ±13	69 ± 13	−9 ± 74	191 ± 80 (1.5 ± 0.6)
Ronne	338,887	156.1 ± 10	59.3 ± 11	149.2 ± 22	−47.4 ± 22	113.5 ± 35 (0.3 ± 0.1)
Ferrigno	117	11.2 ± 1	0.16 ± 0	6.6 ± 2	−0.3 ± 0	5.1 ± 2 (43.4 ± 17)
Venable	3,194	14.6 ± 2	3.5 ± 1	6.5 ± 1	−7.7 ± 1	19.4 ± 2 (6.1 ± 0.7)
Abbot	29,688	34.0 ± 4	25.0 ± 5	2.4 ± 0.5	4.7 ± 18	51.8 ± 19 (1.7 ± 0.6)
Cosgrove	3,033	5.2 ± 1	1.5 ± 0.3	1.3 ± 1.2	−3.1 ± 2	8.5 ± 2 (2.8 ± 0.7)
Pine Island	6,249	126.4 ± 6	4.6 ± 0.9	62.3 ± 5	−33.2 ± 2	101.2 ± 8 (16.2 ± 1)
Thwaites	5,499	113.5 ± 4	4.8 ± 0.9	54.5 ± 5	−33.7 ± 3	97.5 ± 7 (17.7 ± 1)
Crosson	3,229	27.4 ± 2	3.7 ± 0.7	11.7 ± 2	−19.2 ± 1	38.5 ± 4 (11.9 ± 1)
Dotson	5,803	28.4 ± 3	5.7 ± 1	5.5 ± 0.7	−16.6 ± 2	45.2 ± 4 (7.8 ± 0.6)
Getz	34,018	96.7 ± 5	34.2 ± 7	53.5 ± 2	−67.6 ± 12	144.9 ± 14 (4.3 ± 0.4)
Land	640	14.5 ± 1	0.8 ± 0.1	12.2 ± 1	−0.7 ± 0.3	3.8 ± 1 (5.9 ± 2)
Nickerson	6,495	7.8 ± 1	4.6 ± 0.9	4.3 ± 0.6	3.9 ± 1	4.2 ± 2 (0.6 ± 0.3)
Sulzberger	12,333	15.1 ± 2	8.2 ± 2	1.0 ± 0.2	4.1 ± 2	18.2 ± 3 (1.5 ± 0.3)
Swinburne	900	4.9 ± 0.4	0.9 ± 0.2	1.5 ± 0.3	0.6 ± 0.2	3.8 ± 0.5 (4.2 ± 0.6)
Withrow	632	1.3 ±0.2	0.3 ± 0.0	1.2 ± 0.3	0.1 ± 0.1	0.3 ± 0.4 (0.5 ± 0.6)
Ross West	306,105	73.0 ± 4	33.5 ± 6	100.4 ± 8	7.6 ± 17	−1.4 ± 20 (0.0 ± 0.1)
West Antarctica	756,822	730 ± 47	191 ± 36	494 ± 57	−208 ± 36	654 ± 89 (0.9 ± 0.1)
Ross East	194,704	56.1 ± 4	31.0 ± 6	45.9 ± 4	−7.8 ± 11	49.1 ± 14 (0.3 ± 0.1)
Drygalski	2,338	9.6 ± 0.6	0.3 ± 0.1	3.0 ± 1	−0.8 ± 0.4	7.6 ± 1 (3.3 ± 0.5)
Nansen	1,985	1.3 ± 0.5	0.3 ± 0.1	0.2 ± 0.1	0.4 ± 0.1	1.1 ± 0.6 (0.6 ± 0.3)
Aviator	785	1.1 ± 0.2	0.2 ± 0.	0.2 ± 0.1	−0.3 ± 0.1	1.4 ± 0.2 (1.7 ± 0.3)
Mariner	2,705	2.5 ± 0.4	1.1 ± 0.2	0.6 ± 0.2	0.6 ± 0.3	2.4 ± 0.6 (0.9 ± 0.2)
Lillie	770	3.6 ± 0.3	0.2 ± 0.	0.5 ± 0.1	0.0 ± 0.	3.4 ± 0.3 (4.4 ± 0.4)
Rennick	3,273	4.8 ± 1	0.7 ± 0.1	0.8 ± 0.2	−2.3 ± 0.9	7.0 ± 1 (2.2 ± 0.3)
Cook	3,462	36.0 ± 3	1.7 ± 0.3	27.6 ± 3	5.5 ± 1	4.6 ± 5 (1.3 ± 1)
Ninnis	1,899	27.6 ±2	1.3 ± 0.2	24.6 ± 3	2.0 ± 0.9	2.2 ± 3 (1.2 ± 2)
Mertz	5,522	20.0 ± 1	3.6 ± 0.7	12.0 ± 2	3.6 ± 1	7.9 ± 3 (1.4 ± 0.6)
Dibble	1,482	12.5 ± 1	1.5 ± 0.3	8.2 ± 0.9	−2.3 ± 0.7	8.1 ± 1 (5.5 ± 0.9)
Holmes	1,921	26.0 ± 2	2.8 ± 0.5	24.7 ± 4	−2.5 ± 1	6.7 ± 4 (3.5 ± 2)
Moscow Univ.	5,798	52.3 ± 1	4.7 ± 0.9	29.6 ± 3	−0.1 ± 3	27.4 ± 4 (4.7 ± 0.8)
Totten	6,032	71.0 ± 3	6.2 ± 1	28.0 ± 2	−14.0 ± 2	63.2 ± 4 (10.5 ± 0.7)
Vincennes	935	12.7 ± 1	0.5 ± 0.1	6.8 ± 1	1.3 ± 0.6	5.0 ± 2 (5.3 ± 2)
Conger/Glenzer	1,547	1.7 ± 0.4	0.9 ± 0.2	1.1 ± 0.8	−2.1 ± 1	3.6 ± 1 (2.3 ± 0.9)
Tracy/Tremenchus	2,845	0.6 ±0.4	1.0 ± 0.2	0.2 ± 0.1	−1.7 ± 2	3.0 ± 2 (1.5 ± 0.7)
Shackleton	26,080	55.0 ± 4	16.2 ± 3	30.3 ± 3	−31.7 ± 14	72.6 ± 15 (2.8 ± 0.6)
West	15,666	41.9 ± 4	6.9 ± 1	32.6 ± 7	−11.1 ± 7	27.2 ± 10 (1.7 ± 0.7)
Publications	1,551	5.8 ± 0.8	0.4 ± 0.1	5.2 ± 1	−0.5 ± 0.8	1.5 ± 2 (1.0 ± 1)
Amery	60,654	56.0 ± 0.5	8.5 ± 2	50.4 ± 8	−21.4 ± 21	35.5 ± 23 (0.6 ± 0.4)
Wilma/Robert/Downer	858	10.3 ±0.5	0.6 ± 0.1	0.8 ± 0.4	0.0 ± 0	10.0 ± 0.6 (11.7 ± 0.7)
Edward VIII	411	4.1 ± 0.8	0.4 ± 0.1	0.3 ± 0.1	0.0 ± 0	4.2 ± 0.8 (10.2 ± 2)

continued on next page

Table 1 continued

Name	Area km^2	GL Gt/year	SMB Gt/year	Ice front Gt/year	$\partial H/\partial t$ Gt/year	Basal melt Gt/year (m/year)
Edward VIII	411	4.1 ± 0.8	0.4 ± 0.1	0.3 ± 0.1	0.0 ± 0	4.2 ± 0.8 (10.2 ± 2)
Rayner/Thyer	641	14.2 ± 1	0.3 ± 0.1	7.8 ± 0.6	0.0 ± 0	6.7 ± 1 (10.5 ± 2)
Shirase	821	15.0 ± 1	0.4 ± 0.1	9.6 ± 1	0.0 ± 0	5.7 ± 1 (7.0 ± 2)
Prince Harald	5,392	8.3 ± 1	4.1 ± 0.8	10.3 ± 2	4.0 ± 2	−2.0 ± 3 (-0.4 ± 0.6)
Baudouin	32,952	22.0 ± 3	8.4 ± 2	6.5 ± 1	9.8 ± 11	14.1 ± 12 (0.4 ± 0.4)
Borchgrevink	21,580	19.6 ± 3	6.1 ± 1	17.5 ± 3	0.7 ± 4	7.5 ± 6 (0.3 ± 0.3)
Lazarev	8,519	3.7 ± 0.6	2.0 ± 0.4	3.1 ± 1	−3.6 ± 2	6.3 ± 2 (0.7 ± 0.2)
Nivl	7,285	3.9 ± 0.8	1.8 ± 0.3	1.3 ± 0.4	0.6 ± 1	3.9 ± 2 (0.5 ± 0.2)
Vigrid	2.089	2.7 ± 0.4	0.4 ± 0.1	2.0 ± 0.4	−2.0 ± 0.4	3.2 ± 0.7 (1.5 ± 0.3)
Fimbul	40,843	24.9 ± 4	12.7 ± 2	18.2 ± 2	−4.0 ± 7	23.5 ± 9 (0.6 ± 0.2)
Jelbart	10,844	9.9 ± 1	4.9 ± 0.9	8.8 ± 2	6.9 ± 2	−1.0 ± 3 (-0.1 ± 0.3)
Atka	1,969	0.9 ± 0.2	0.8 ± 0.1	1.0 ± 0.2	1.1 ± 0.2	−0.5 ± 0.4 (-0.2 ± 0.2)
Ekstrom	6,872	4.1 ± 0.8	2.6 ± 0.5	2.3 ± 0.6	0.0 ± 0	4.3 ± 2 (0.6 ± 0.2)
Quar	2,156	1.0 ±0.2	0.5 ± 0.1	0.6 ± 0.1	−0.5 ± 0.4	1.4 ± 0.5 (0.7 ± 0.2)
Riiser-Larsen	43,450	21.5 ± 3	12.7 ± 2	12.1 ± 2	13.4 ± 8	8.7 ± 9 (0.2 ± 0.2)
Brunt/Stancomb	36,894	20.3 ± 3	11.4 ± 2	28.1 ± 4	2.6 ± 4	1.0 ± 7 (0.03 ± 0.2)
Filchner	104,253	97.7 ± 6	13.4 ± 2	82.8 ± 4	−13.6 ± 7	41.9 ± 10 (0.4 ± 0.1)
East Antarctica	669,781	782 ± 80	174 ± 33	546 ± 70	−70 ± 34	480 ± 116 (0.7 ± 0.2)
Total surveyed	**1,553,978**	**1,696 ± 146**	**430 ± 81**	**1,089 ± 139**	**−287 ± 89**	**1,325 ± 235 (0.85 ± 0.1)**
Total Antarctica	1,561,402	2,048 ± 149		1,265 ± 141		1,500 ± 237

The total ice-shelf grounding-line inflow of 1696 ± 146 Gt/year combined with an *SMB* input of 430 ± 81 Gt/year is partitioned into an ice-front flux of 1,089 ± 139 Gt/year and a basal meltwater production of 1,325 ± 235 Gt/year. Basal melting thus accounts for 55 ± 10% of ice-shelf mass ablation. The corresponding area-average melt rate of 85 ± 15 cm/year is three times as large as the average *SMB* on ice shelves (28 ± 5 cm) and five times the average *SMB* on grounded ice sheet (16 ± 1 cm) (*16*), illustrating the considerable importance of ocean interactions in freshwater transfers between the ice and ocean.

The grounding-line flux of all surveyed ice shelves accounts for 83 ± 7% of the total ice discharge into the Southern Ocean (Table 1). Total Antarctic grounded ice discharge (*26*) is 352 ± 30 Gt/year higher than our grounding-line flux because of additional discharge from smaller ice shelves and ice walls that terminate in the ocean (*27*). An equal partitioning of these missing areas between calving and basal melting (see supplementary materials) would increase in situ meltwater production to 1500 ± 237 Gt/year and ice-front flux to 1265 ± 139 Gt/year.

The comparison of basal melting B (Fig. 1) with steady state melting B_{ss} (fig. S4, Table 1, and table S1) shows that many ice shelves are near equilibrium ($B \sim B_{ss}$), whereas some are thickening ($B < B_{ss}$) and others are thinning ($B > B_{ss}$). High basal melting is therefore not synonymous with thinning. Ice shelves with high melt rates can be in a state of mass balance, but meltwater production is 28 ± 9% higher than required to maintain the ice shelves in overall steady state (1037 ± 218 Gt/year). Ice shelves in the Amundsen Sea sector (Pine Island to Getz) contribute 59% of the 287 ± 89 Gt/year imbalance, an attrition rate twice that of their glacier source regions over the same time period (*26*). Similarly, the total imbalance of all Antarctic ice shelves combined is more than twice that of the grounded ice (*26*).

The ratio of calving to melting averages 0.45 ± 0.3, but exhibits considerable regional variability (Table 1), with area-average melt rates varying from negative to > 40 m/year. This wide range reflects diverse ocean environments, which include seawater temperature, the depths of troughs and sills that influence the access of oceanic heat to ice-shelf cavities, and the sea-ice formation and drifts resulting from atmospheric forcing.

Large ice shelves generate a disproportionally small portion of the total ice-shelf meltwater despite high production rates in their deep grounding zones and along lengthy ice fronts. The four giants with areas >100,000 km^2 (Ross East, Ross West, Filchner, and Ronne) cover 61% of the total ice-shelf area but contribute only 15% of the meltwater at an average rate of 13 cm/year. The low melt rates result from the relatively weak ocean heat source provided by cold shelf waters, in turn leading to substantial marine ice accretion (*28*). Despite areas 3 to 10 times as large as the Getz, none of the big four ice shelves produce as much meltwater, with the Ross West contributing no net melt. Meltwater from the Southeast Pacific-Antarctic sector (George VI through Getz) accounts for 48% of the total meltwater over only 8% of the area, with the Getz being the largest meltwater source in Antarctica during the study period. B averages 5.1 m/year in this region, from a maximum of 43 m/year under the short Ferrigno Glacier tongue to a minimum of 1.8 m/year beneath the Abbot. That area-average rate may seem low for a warm-cavity Southeast Pacific ice shelf, but the moderate-sized, shallow-draft Abbot (*29*) ranks eighth overall in meltwater production, while maintaining a positive mass balance ($B < B_{ss}$).

Meltwater production from several small East Antarctic ice shelves in the Wilkes Land sector is larger than expected. Area-average melt rates from Dibble through Vincennes (4 to 11 m/year) are comparable to Amundsen Sea ice-shelf rates from Crosson through Land (4 to 11 m/year), whereas meltwater produced by Shackleton and West (73 and 27 Gt/year, respectively) rivals that from Thwaites and Sulzberger (98 and 18 Gt/year, respectively). Except for the region from 140° to 150°W where Mertz and Ninnis melting is dominated by shelf waters, oceanographic data are sparse along the Wilkes Land coastline. "Modified" warm deep water at a temperature near 0°C has been reported 40 km south of the continental shelf break northeast of Totten (*30*). By analogy with observations in the Amundsen Sea, our results suggest the presence of seawater at similar temperatures under several East Antarctic ice shelves. Even 0° seawater at outer continental shelf depths could expose ice shelves with deep grounding lines like the Totten (2.2 km), Moscow (2.0 km), and Shackleton (1.8 km) to temperatures more than 3°C above their melting points. To evaluate the impact of these warm deep waters on ice-shelf melting, more information is needed about their spatial and temporal variability on the outer shelf and links through glacially scoured troughs to the vulnerable glacier grounding lines.

Our glaciological estimates are generally consistent with recent results from high-resolution ocean models in the Amundsen, Bellingshausen,

and Weddell Seas (*29*, *31*–*33*) (see supplementary materials), but total melting of 10 of the larger ice shelves is notably less here than in circumpolar models (*7*, *11*). Discrepancies between model results and observations have been attributed to deficiencies in atmospheric forcing, the representation of sea-ice cover, the smoothing of bottom topography, and assumptions regarding cavity shape. Some models yield annual cycles and decadal variability (*29*) that can now be compared for specific periods with glaciological measurements, which need to be extended in time.

Our results indicate that basal melting accounts for a larger fraction of Antarctic ice-shelf attrition than previously estimated. These improved glaciological estimates provide not only more accurate and detailed reference values for modeling but also a baseline for similar future studies. Ice-shelf meltwater production exhibits a complex spatial pattern around the continent, with an outsized contribution of smaller, fast-melting ice shelves in both West and East Antarctica. Warm-cavity ice shelves along the Southeast Pacific coastline, predicted and observed to be sensitive to ocean warming and circulation strength (*9*, *34*), were thinning rapidly in 2003 to 2008 (*23*). Nearly half of the East Antarctic ice shelves were also thinning, some due to probable exposure to "warm" seawater, with connections to ice drainage basins grounded below sea level.

Continued observations of ice-shelf velocity and thickness change, along with more detailed information on cavity shape, seafloor topography, and atmospheric and oceanic forcing variability are critical to understand the temporal variability and evolution of Antarctic ice shelves. Continued warming of the ocean will slowly increase ice-shelf thinning, but if major shifts in sea ice cover and ocean circulation tip even large ice-shelf cavities from cold to warm (*35*), there could be major changes in ice shelf and thus ice-sheet mass balance.

References and Notes

1. P. Fretwell *et al.*, *The Cryosphere* **7**, 375–393 (2013).
2. C. W. Swithinbank, *Satellite Image Atlas of Glaciers of the World: Antarctica*, R. S. Williams, J. G. Ferrigno, Eds. (USGS Prof. Paper 1386-B, 1988).
3. N. I. Barkov, *Ice Shelves of Antarctica* (New Delhi, NY, Amerind Publishing Company, 1985).
4. R. LeB. Hooke, *Principles of Glacier Mechanics* (Cambridge University Press, Cambridge, 2005).
5. K. M. Cuffey, W. S. B. Paterson, *The Physics of Glaciers* (Elsevier, Burlington, MA, ed. 4, 2010).
6. S. S. Jacobs *et al.*, *J. Glaciol.* **38**, 375 (1992).
7. H. H. Hellmer, *Geophys. Res. Lett.* **31**, L10307 (2004).
8. A. Jenkins, S. S. Jacobs, *J. Geophys. Res.* **113**, (C4), C04013 (2008).
9. S. S. Jacobs, A. Jenkins, C. F. Giulivi, P. Dutrieux, *Nature Geosci.* **4**, 519–523 (2011).
10. A. Foldvik, T. Gammelsrod, E. Nygaard, S. Osterhus, *J. Geophys. Res. Oceans* **106**, 4463 (2001).
11. R. Timmermann, Q. Wang, H. H. Hellmer, *Ann. Glaciol.* **53**, 303–314 (2012).
12. I. Joughin, L. Padman, *Geophys. Res. Lett.* **30**, 1477 (2003).
13. J. Wen *et al.*, *J. Glaciol.* **56**, 81–90 (2010).
14. E. Rignot, S. S. Jacobs, *Science* **296**, 2020–2023 (2002).
15. A. Jenkins, C. S. M. Doake, *J. Geophys. Res.* **96**, 791 (1991).
16. J. T. M. Lenaerts *et al.*, *J. Geophys. Res.* **117**, D05108 (2012).
17. E. Rignot *et al.*, *Nat. Geosci.* **1**, 106–110 (2008).
18. C. Allen, IceBridge MCoRDS L2 Ice Thickness. Boulder, Colorado, USA: NASA DAAC at the National Snow and Ice Data Center (2010).
19. D. D. Blankenship, S. Kempf, D. Young, IceBridge HiCARS 2 L2 Geolocated Ice Thickness. Boulder, Colorado, USA: NASA DAAC at the National Snow and Ice Data Center (2012).
20. J. A. Griggs, J. L. Bamber, *J. Glaciol.* **57**, 485–498 (2011).
21. E. Rignot, J. Mouginot, B. Scheuchl, *Geophys. Res. Lett.* **38**, L10504 (2011).
22. E. Rignot, J. Mouginot, B. Scheuchl, *Science* **333**, 1427–1430 (2011).
23. H. D. Pritchard *et al.*, *Nature* **484**, 502–505 (2012).
24. K. Makinson *et al.*, *Geophys. Res. Lett.* **38**, L06601 (2011).
25. H. J. Horgan, R. T. Walker, S. Anandakrishnan, R. B. Alley, *J. Geophys. Res.* **116**, C02005 (2011).
26. A. Shepherd *et al.*, *Science* **338**, 1183–1189 (2012).
27. S. Neshyba, E. G. Josberger, *J. Phys. Oceanogr.* **10**, 1681–1685 (1980).
28. K. Grosfeld *et al.*, *Antarct. Res. Ser.* **75**, 319–339 (1998).
29. M. P. Schodlok, D. Menemenlis, E. Rignot, M. Studinger, *Ann. Glaciol.* **53**, 156–162 (2012).
30. G. D. Williams *et al.*, *Deep Sea Res. Part II Top. Stud. Oceanogr.* **58**, 1194–1210 (2011).
31. P. R. Holland, A. Jenkins, D. Holland, *Geophys. Res. Lett.* **115**, (C5), C05020 (2010).
32. L. Padman *et al.*, *J. Geophys. Res.* **117**, C01010 (2012).
33. P. R. Holland *et al.*, *Geophys. Res. Lett.* **36**, L11604 (2009).
34. P. R. Holland, A. Jenkins, D. M. Holland, *J. Clim.* **21**, 2558–2572 (2008).
35. H. H. Hellmer *et al.*, *Nature* **485**, 225–228 (2012).

Acknowledgments: We thank three anonymous reviewers for their constructive criticism of the manuscript. This work was performed at the University of California, Irvine, and at the Jet Propulsion Laboratory, California Institute of Technology, under grants from NASA's Cryospheric Science Program and Operation IceBridge (OIB) and at the Lamont-Doherty Earth Observatory of Columbia University under grants from the National Science Foundation and the National Oceanic and Atmospheric Administration.

Supplementary Materials

www.sciencemag.org/cgi/content/full/science.1235798/DC1
Supplementary Text
Figs. S1 to S4
Tables S1 and S2
References (*36*–*58*)

29 January 2013; accepted 31 May 2013
Published online 13 June 2013;
10.1126/science.1235798

Lethal Aggression in Mobile Forager Bands and Implications for the Origins of War

Douglas P. Fry[1,2]* and Patrik Söderberg[1,3]

It has been argued that warfare evolved as a component of early human behavior within foraging band societies. We investigated lethal aggression in a sample of 21 mobile forager band societies (MFBS) derived systematically from the standard cross-cultural sample. We hypothesized, on the basis of mobile forager ethnography, that most lethal events would stem from personal disputes rather than coalitionary aggression against other groups (war). More than half of the lethal aggression events were perpetrated by lone individuals, and almost two-thirds resulted from accidents, interfamilial disputes, within-group executions, or interpersonal motives such as competition over a particular woman. Overall, the findings suggest that most incidents of lethal aggression among MFBS may be classified as homicides, a few others as feuds, and a minority as war.

A controversy exists regarding mobile forager band societies (MFBS) and warfare. Field researchers who have worked with MFBS generally report that warfare is absent or rudimentarily developed (*1*–*6*). Fry (*7*) compared MFBSs with complex and equestrian foragers and found that most MFBS (62%) were nonwarring, whereas all of the complex and equestrian societies made war. On the other hand, Wrangham and Glowacki [(*8*), p. 7] developed a chimpanzee-based lethal raiding model, asserting that "humans evolved a tendency to kill members of other groups," and they provided ethnographic quotations on MFBS to illustrate the model. They [(*8*), p. 8] define war as when "coalitions of members of a group seek to inflict bodily harm on one or more members of another group; 'groups' are independent political units." Bowles (*9*) examined war deaths in eight societies, six of which were MFBS, and reported the occurrence of war in all eight societies, which he takes as confirmation that war has been pervasive during human evolution.

[1]Peace, Mediation and Conflict Research, Åbo Akademi University in Vasa, Post Office Box 311, FIN-65101, Vasa, Finland. [2]Bureau of Applied Research in Anthropology, School of Anthropology, Post Office Box 210030, Tucson, AZ 85721–0030, USA. [3]Developmental Psychology, Åbo Akademi University in Vasa, Post Office Box 311, FIN-65101, Vasa, Finland.

*Corresponding author. E-mail: dfry@abo.fi